physica status solidi a
www.pss-a.com

Analysis of Optical Potential and Electrical Loss between Upright Pyramids and Inverted Pyramids on Silicon Heterojunction Solar Cells

Daxue Du, Dongting Ye, and Wenzhong Shen**

Several studies have demonstrated that inverted pyramid (IP) structures confer significant advantages over upright pyramid (UP) designs in silicon solar cells. Nevertheless, the most notable efficiency records of the past decades have been predominantly set using UP configurations, rather than IP structures. Herein, both UP and IP structures are fabricated to assess their performance on wafer and silicon heterojunction (SHJ) solar cells. The optical benefits of IP structures on wafers are drastically curtailed when applied on SHJ solar cells due to the introduction of front antireflective films, as also verified through optical simulations. Additionally, the IP textured device exhibits a 3.35% efficiency difference compared to the UP textured one, attributed to enhanced surface recombination, higher series resistance, and lower shunt resistance. Furthermore, optical simulations suggest that substrate thickness hardly impacts the preference for UP or IP structures after normalizing the sizes and tilt angles, while the incident angle and rear reflective layer are critical factors. Quokka 2 and Wafer Ray Tracer are used for optical and electrical simulations, respectively.

1. Introduction

Crystalline silicon (c-Si) solar cells have consistently dominated the global photovoltaic market owing to their high efficiency, abundant materials, mature technology, and superior stability.[1,2] The enhancement of optical absorption in c-Si solar cells is largely achieved through the incorporation of light-trapping structures, which contribute significantly to power conversion efficiency (PCE).[3] One of the most established light-trapping strategies is the fabrication of micro upright pyramids (UP) using alkali etching techniques.[3–8] Various textured structures have been explored to minimize device reflection losses,[9] with inverted pyramid (IP) emerging as a viable alternative to UP structures in industrial applications owing to the multiple trap light effect.[10–15]

The widespread interest in IP structures stems from the pioneering work of Martin's team, who achieved over 24% PCE in silicon solar cells during the 1990s.[16,17] Recently, Tong et al. reported that IP structures offer superior antireflection properties but poorer surface passivation compared to UP, resulting in a lower PCE.[18] Sun et al. have successfully fabricated silicon heterojunction (SHJ) solar cells with both UPs and IPs by regulating the concentration of the nucleating agent, with IPs achieving a PCE gain of 0.2%.[19] Although most studies highlight the benefits of IP structures in enhancing device efficiency relative to UP structures,[20–25] few researchers have provided a direct comparison between UP and IP devices while controlling for other experimental variables. Given the difficulty in precisely controlling the size of UP and IP structures in physical experiments, optical simulations have emerged as a promising tool for such comparisons.[26,27] Furthermore, there is a lack of comprehensive studies addressing the discrepancies between experimental results and idealized simulations, which is crucial for optimizing IP structures.

Additionally, silicon consumption is a key cost consideration in solar cells, prompting the development of solar technologies that are compatible with thinner wafers.[28–30] Due to the low-temperature process and highly symmetric structure, large-area SHJ solar cells have recently been validated to perform effectively with substrates as thin as 50–60 μm.[7,8] Consequently, the ability of IP structures to perform on thin solar cells is critical in the competition with UP structures. However, there has been limited focus on the rear reflective layer in thin solar cells, which affects the decision of IP versus UP designs.

This work explores the optical and electrical distinctions between UP and IP structures in SHJ solar cells. IPs were fabricated using the metal-assisted chemical etching (MACE) method, which is widely employed for such processes.[31–33] Light-trapping effects were compared to identify optical differences between the two structures both on wafer and complete device.

D. Du, D. Ye
Shanghai Hency Solar Technology Co., Ltd
Shanghai 201109, P. R. China
E-mail: dudx@shanghai-electric.com

D. Du, D. Ye
Shanghai Electric Group Hency Solar Technology (Nantong) Co., Ltd
Nantong 226100, P. R. China

W. Shen
Institute of Solar Energy, School of Physics and Astronomy
Shanghai Jiao Tong University
Shanghai 200240, P. R. China
E-mail: wzshen@sjtu.edu.cn

The ORCID identification number(s) for the author(s) of this article can be found under https://doi.org/10.1002/pssa.202500220.

DOI: 10.1002/pssa.202500220

External quantum efficiency (EQE) measurements were used to quantify the optical gain when considering surface recombination. The limitations of IP structures in terms of short-circuit current density (J_{SC}), open-circuit voltage (V_{OC}), and filling factor (FF) were observed from J–V curve measurements and analyzed further using free energy loss through Quokka 2 software. Moreover, optical simulations were performed to investigate the potential of IPs under varying incident angles, substrate thicknesses, and rear reflective layers.

2. Experimental Section

2.1. Surface Texturization

Phosphorus-doped monocrystalline silicon wafers with a thickness of 150 μm were polished in a 10 wt% NaOH solution at 80 °C for 3 min to remove saw damage. The polished wafers were subsequently treated in a 5 wt% NaOH solution with added isopropanol at 80 °C for 10 min, resulting in bifacial UPs. IPs were fabricated using the MACE method. The wafers were immersed in a mixed solution of 0.1 mM $AgNO_3$ and 0.5 M HF for 30 s, facilitating the deposition of randomly distributed Ag nanoparticles. The substrates were then placed into a 1.5 M HF and 0.5 M H_2O_2 solution for 30 min to form a textured surface, followed by modification in a 2 wt% NaOH solution to achieve the IP structures. The schematic structure of a silicon wafer after UP and IP texturing is shown in **Figure 1**a.

2.2. Device Fabrication

As depicted in Figure 1b, the intrinsic typed hydrogenated amorphous silicon (i:a-Si:H) films with 5 nm were bifacially deposited on the textured wafer via the plasma-enhanced chemical vapor deposition method. Subsequently, 5 nm of phosphorus-doped hydrogenated amorphous silicon (n:a-Si:H) was deposited on the front side, and 15 nm of boron-doped hydrogenated amorphous silicon (p:a-Si:H) was deposited on the rear side. Then, the substrate was prepared by physical vapor deposition on both sides with a transparent conductive film of indium tin oxide. Finally, Ag grids were formed using the screen-printing technique, followed by annealing at 200 °C.

2.3. Optical and Electrical Simulations

Wafer Ray Tracer was utilized to model the light-trapping schemes of UPs and IPs in SHJ solar cells.[34] The AM1.5G spectrum was introduced as the incident light source, and the refractive indices and extinction coefficients of the materials in the SHJ solar cell were taken from the PV Lighthouse database.[35] The UP and IP structures were defined with identical geometric dimensions based on the prepared UPs: a height of 1.5 μm, a width of 2.1 μm, and a texture angle of 54.7°. The shading effects caused by the metal electrodes were not accounted for in the simulations.

The reflection, transmission, and absorption spectra for the wafer and SHJ solar cells were calculated within the 300–1200 nm wavelength range. The maximum generated current density (J_G) is determined by assuming an internal quantum efficiency (IQE) of 100%, as shown in Equation (1):[36]

$$J_G = \frac{q}{hc}\int_{300}^{1200} A(\lambda)\mathrm{IQE}(\lambda)\varnothing(\lambda)\lambda \mathrm{d}\lambda \quad (1)$$

where q is the electron charge, $\varnothing(\lambda)$ is the standard spectral photon density of AM1.5G spectrum, and $A(\lambda)$ represents the absorption spectrum of the active layer. Various optical losses were then converted into current densities using Equation (1) for a quantitative comparison, including external reflection ($J_{R,ext}$), escape reflection ($J_{R,esc}$), transmission (J_T), parasitic absorption of front films ($J_{A,F}$), and rear films ($J_{A,R}$). The external and escape reflections represent reflected light that does not and does enter the interior of the devices, respectively.

We analyzed recombination and resistance losses by simulating the effects of various textured surfaces on the electrical properties of SHJ solar cells and performing free energy loss analysis (FELA) using Quokka 2 software.[37,38] The variables of saturated dark current density, contact resistivity, and the external series and shunt resistances illustrate the influence of UPs and IPs on electrical performance. The key input parameters for the Quokka 2 simulations are listed in Table S1, Supporting Information.

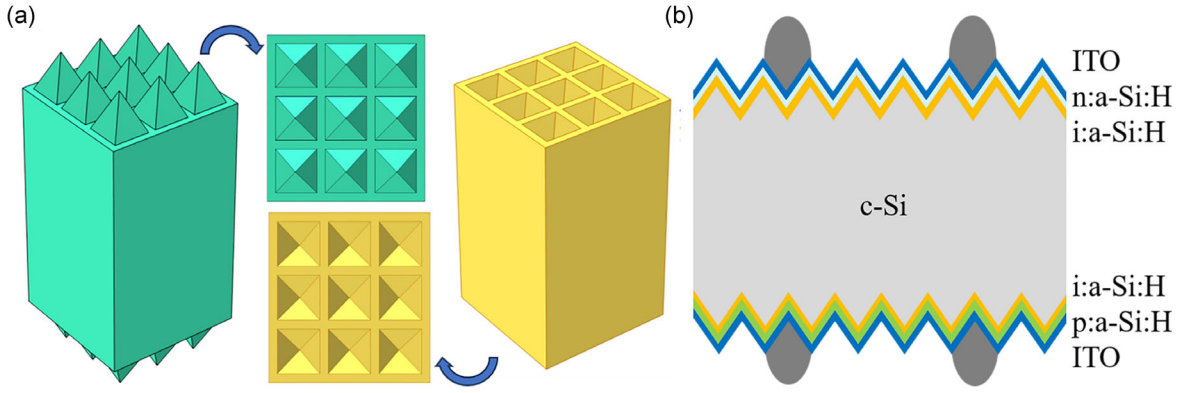

Figure 1. a) Main and top views of UP and IP textured silicon wafers. b) The schematic structure of SHJ solar cell.

3. Results and Discussion

3.1. Antireflection between Wafers and Devices

Figure 2a presents the schematic diagrams of double bounce for UPs and triple bounce for IPs, excluding photon volatility.[25] Ray tracing at normal incidence reveals that UPs trap light twice through multiple pyramid interactions, while IPs rely on the internal structure of a single pyramid to achieve three light traps. Figure 2b–c displays SEM images of the UP and IP structures on monocrystalline silicon wafers, textured by the alkali etching and MACE methods, respectively. It can be observed that the sizes of the random UPs are estimated to be about 2 μm, while the sizes of IPs are distributed from 0.5 to 1 μm.

As shown in Figure 2d, reflection spectra are presented for different textured surfaces in a wavelength ranging from 400 to 1100 nm, where IP structures exhibit a 5% antireflective gain across nearly the entire range. After coating the textured wafers with a-Si:H and ITO films, the SHJ solar cell reflections, compared to the wafer, were significantly suppressed in the 450–1000 nm range. Meanwhile, the minimum reflection shifted from ≈1000 to 600 nm. However, the advantages of IPs in trapping light are significantly diminished, as stacked films with gradient refractive indices also provide antireflection,[39] thus reducing the reflective gap between the textured devices and wafers.

Indeed, discrepancies between the optical properties of simulated and experimental results can be attributed to the irregularities typically found in chemically treated UPs, as evidenced in several studies.[18,31,40] Therefore, we carried out optical simulations to compare the optical performance with UPs and IPs, maintaining consistency in the length, height, and tilt angle.

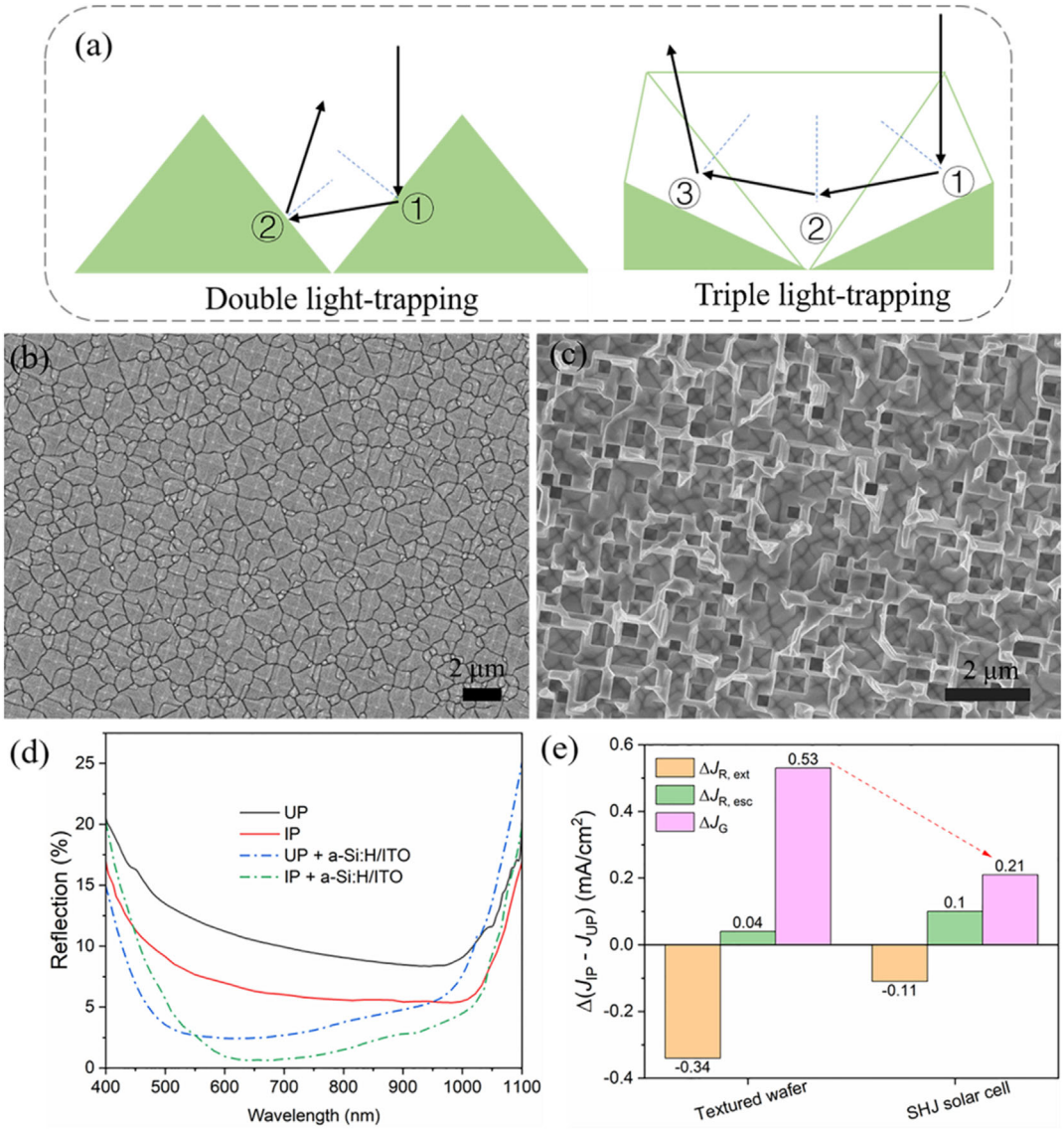

Figure 2. a) Illustrated double light trapping effect for UPs and triple light trapping effect for IPs. SEM images of wafer surface with b) UPs and c) IPs. d) Reflection of UPs and IPs on wafer and SHJ solar cell. e) Current density difference between UPs and IPs on wafer and SHJ solar cell.

Figure 2e illustrates the simulated difference in current density on the wafer between UP and IP configurations. The IP structure exhibits a superior antireflective effect, reducing $J_{R,ext}$ by 0.34 mA cm^{-2} and increasing $J_{R,esc}$ by 0.04 mA cm^{-2} compared to UP structures, leading to a 0.53 mA cm^{-2} gain in J_G. However, when the textured wafers are subsequently coated with a-Si:H and ITO films, the advantage of IP is reduced to 0.21 mA cm^{-2}, as both $\Delta J_{R,ext}$ and $\Delta J_{R,esc}$ are enhanced. These results indicate that comparing the light trapping differences only at the wafer level between UPs and IPs misinterprets their contributions at the devices.

3.2. Photovoltaic Performance with UPs and IPs

To compare the difference in optical recombination loss with UP and IP structures, as inserted in **Figure 3**a, EQE spectra were measured with different textured surfaces. Despite the reflection advantage above 550 nm, the IP structures possess a reduced EQE response compared to UP structures from 300 to 1000 nm, which arises from a decrease in IQE due to the larger surface recombination losses of IPs. Furthermore, we depicted the statistical J–V parameters on different textured surfaces. As shown in Figure 3b, the SHJ solar cell obtains an average J_{SC} loss of 0.86 mA cm^{-2} when applying IPs in place of UPs. Meanwhile, the V_{OC} was observed to be reduced by about 50 mV, which originated from the IP of the adverse surface passivation level.[18] Moreover, the FF of IPs is significantly reduced by nearly 10% compared to UPs due to the deterioration of the series resistance from 2.77 to 4.06 Ω cm^2 and shunt resistance from 14.4 to 0.4 kΩ cm^2 in Figure 3c. Consequently, the average PCE has been significantly reduced from 18.65% to 14.70%, with the champion device with UPs and IPs exhibiting a PCE of 19.54% and 16.19% in Figure 3d. Figure 3e reveals the simulation results of the FELA with UPs and IPs, with significant changes in contact recombinations and external resistances. The shunt resistance resulted in the largest free energy loss gap of 0.86 mW cm^{-2} between UPs and IPs, followed by the

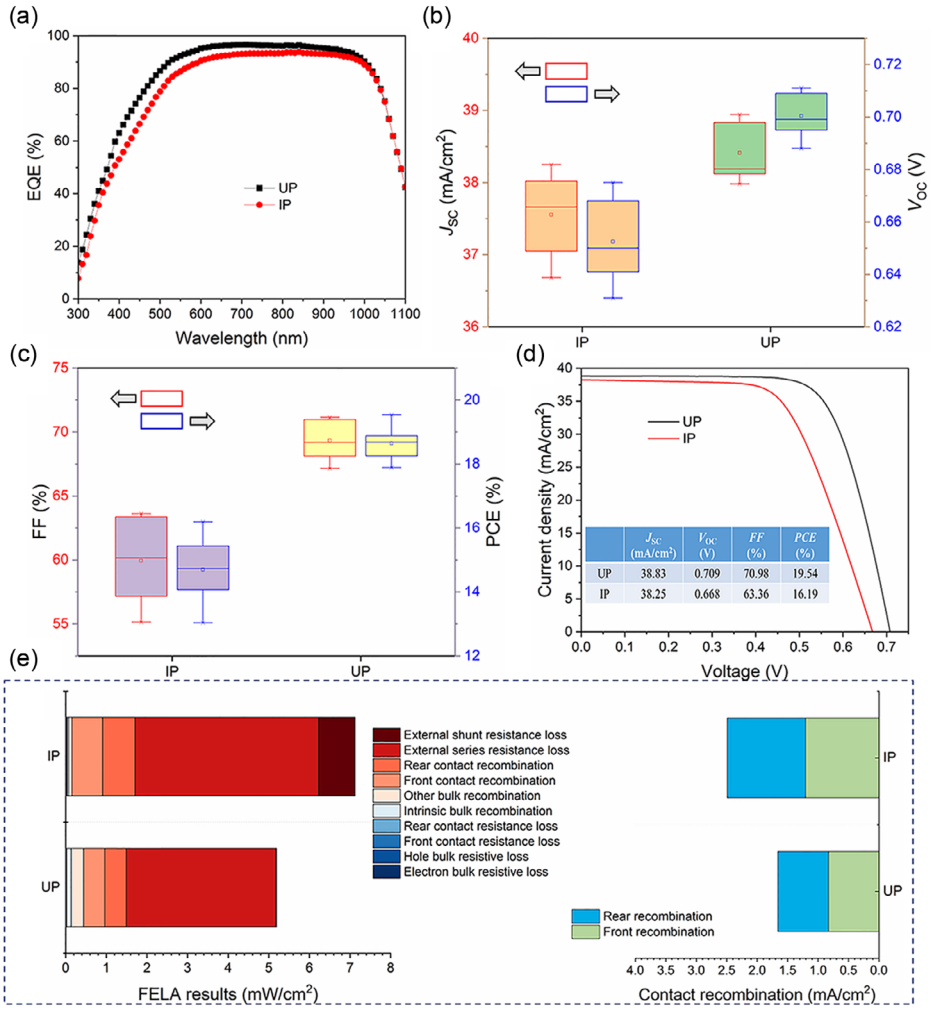

Figure 3. a) EQE curves of SHJ solar cells with UPs and IPs. Statistical photovoltaic performance parameters with different textured surfaces, including b) short-circuit current density and open-circuit voltage, as well as c) FF and efficiency. d) Optimized J–V curves of SHJ solar cells with UPs and IPs. e) FELA and contact recombination current density loss in SHJ solar cells with UPs and IPs.

series resistance of 0.85 mW cm^{-2}. Additionally, the IPs induce a more current density loss of about 0.8 mA cm^{-2} due to the surface recombination effect.

3.3. Dependence of Structure and Incident Angle

Although the IP structures show inferior performance in terms of device passivation and contact, which are expected to improve with future technological advancements, we performed additional optical simulations to examine the absorption and loss spectra in SHJ solar cells and aimed to explore the optical potential of IP structures, as shown in **Figure 4**a–b. After aligning the geometric parameters, UPs and IPs demonstrated similar optical behaviors, in contrast to the findings in Figure 2d. The c-Si active layer exhibits weak light absorption below 500 nm due to high reflection and parasitic absorption by the front films. Above 1000 nm, the absorption decreases sharply due to a reduction in the extinction coefficient, leading to increased transmission and escape reflection. Figure 4c presents the current density corresponding to the optical losses, demonstrating that the differences between UPs and IPs lie in reflection and transmission rather than in parasitic absorptions. As a result, SHJ solar cell with UPs and IPs achieved a J_G of 38.80 and 39.02 mA cm^{-2}, respectively.

Considering that the intensity of sunlight in the outdoor decays with incident angle, Figure 4d plots the change of J_G with increasing incident angle from 0° to 80°. It is evident that for incident angles below 40°, the IP structures gain a J_G advantage over the UP structures, while the situation is reversed at the incident angle larger than 40°. To explore this phenomenon, $J_{R,ext}$, $J_{R,esc}$, and J_T are compared with different incident angle in Figure 4e–f. In general, IPs keep a larger $J_{R,ext}$, smaller $J_{R,exc}$, and smaller J_T as the incident angle increasing from 0° to 40°. However, this trend is altered at angles greater than 40° as the IPs no longer feature a triple light trapping effect, exhibiting a significant increase in $J_{R,ext}$, as well as the downsizing advantages in $J_{R,exc}$ and J_T.

3.4. Optical Differences in Thin Devices

A prominent attraction of SHJ solar cells is compatible with thinner wafers compared to other silicon-based solar cells.[41] Therefore, we investigated the optical performance of UPs and IPs on different substrate thicknesses. As displayed in **Figure 5**a–b, both UPs and IPs are capable of the task of trapping light on substrates as thin as 20 μm. To compensate for the significant transmission losses in the infrared region of thin wafer, a rear reflective layer with a low refractive index is normally employed. Taking wafer thickness of 60 μm as an example, Figure 5c,d plots the infrared absorption spectra for UP- and IP-textured SHJ solar cells, where the absorption is enhanced by Ag, Cu, and Al layers.

The mechanism of the rear reflected layer is revealed in Figure 5e,f. Obviously, with the introduction of the rear metal reflective layer, the photons with a long wavelength are not able to pass through the bottom of the solar cell. As a result, part of these photons is absorbed by the reflective layer, while the remaining portion is reflected back into the device. These reflected photons are subsequently absorbed by the substrate, front films, or escape through the front surface. Despite the UP and IP structures achieving a J_G of 37.54 and

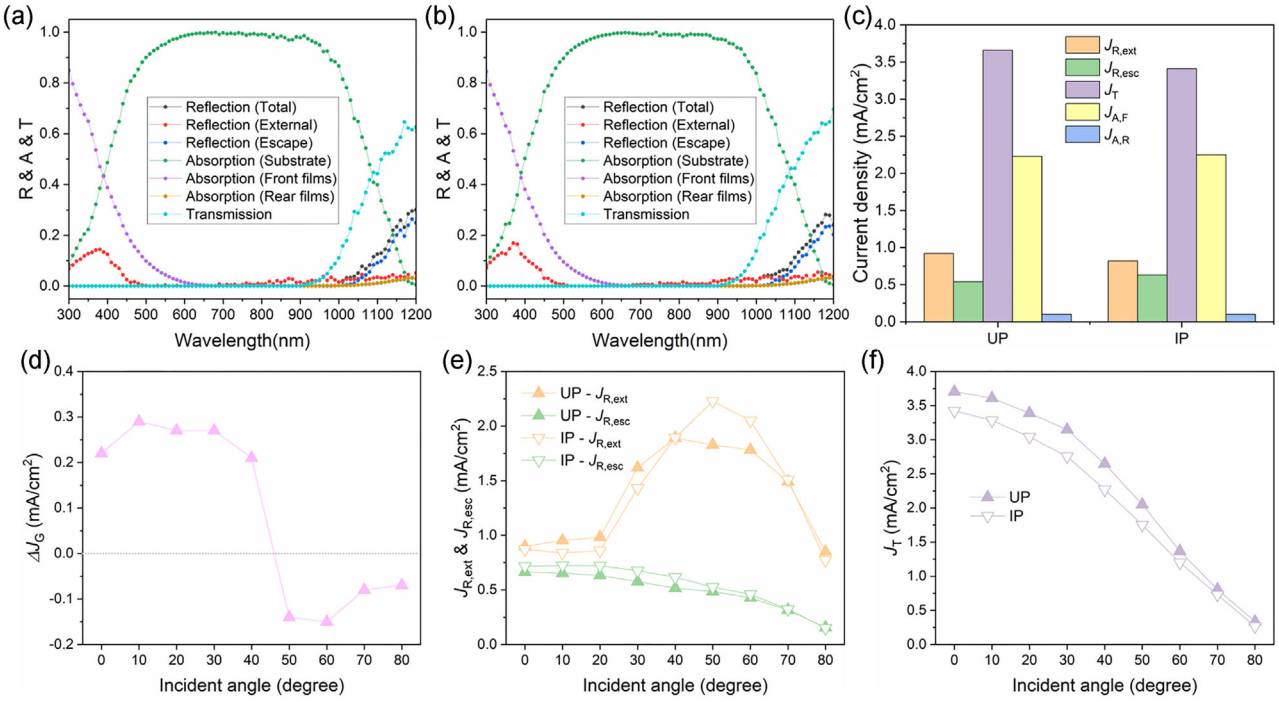

Figure 4. Simulated reflection, absorption, and transmission spectra of SHJ solar cells with a) UP and b) IP structures; c) statistic optical losses of SHJ solar cells with UP and IP structures. d) J_G, e) J_R, and f) J_T of SHJ solar cells with UP and IP structures under different incident angles.

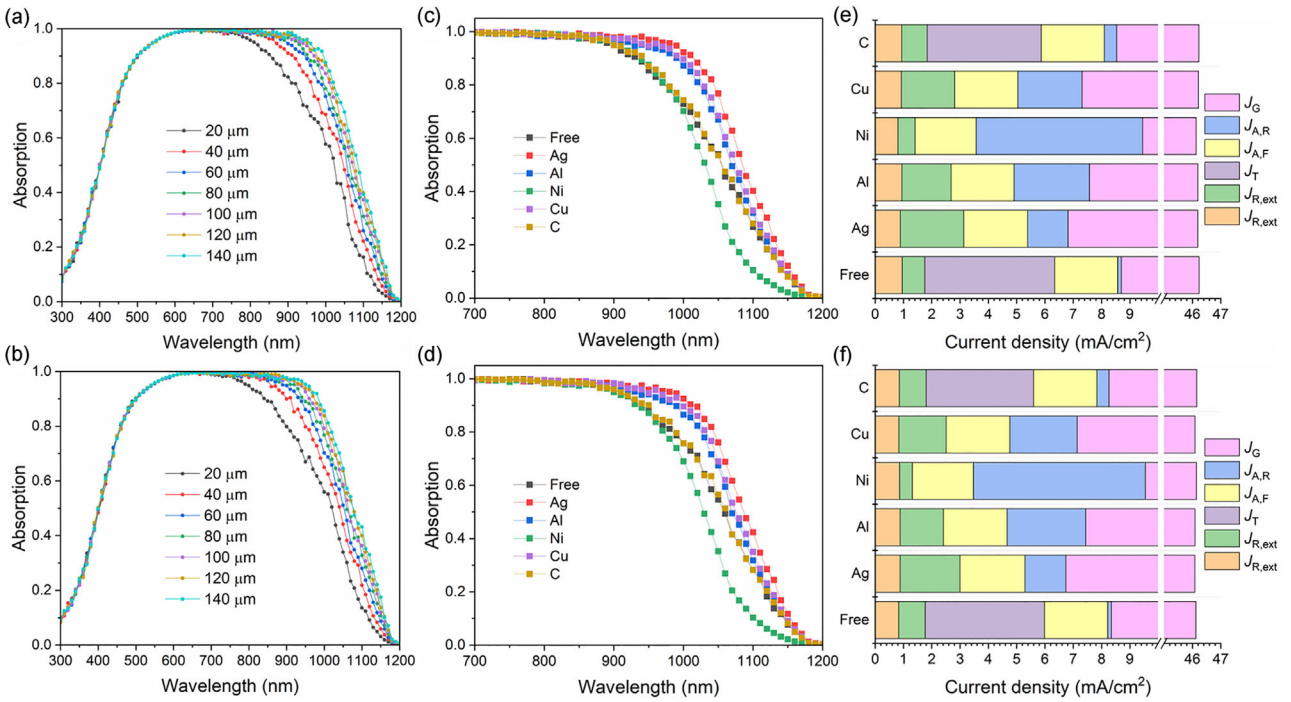

Figure 5. Absorption spectra of a) UP and b) IP textured SHJ solar cells with different wafer thicknesses. Absorption spectra of c) UP and d) IP textured SHJ solar cells with different rear reflection layers with a thickness of 60 μm; current densities corresponding to optical losses of e) UP and f) IP textured SHJ solar cells with different rear reflection layers.

37.78 mA cm^{-2}, respectively, Ag brings the gains of 1.83 and 1.57 mA cm^{-2} in UPs and IPs, which implies that the rear reflected layer also reduces or even reverses the IP-to-UP superiority as does the front reflective layers. Considering the high cost of Ag for applications in the photovoltaic industry,[34,42] Cu and Al are recommended as rear reflective layer alternatives.

4. Conclusions

In conclusion, we have comprehensively assessed the optical and electrical properties of UPs and IPs in SHJ solar cells through a combination of experiments and simulations. IP structures demonstrate optical advantages due to the triple light-trapping effect on wafers, but this advantage is significantly reduced in SHJ solar cells due to the front antireflection films. We found that the fabricated devices with IP structures exhibit lower J_{SC}, V_{OC}, and FF compared to UP structures, which is primarily due to the irregular morphology of the IPs created via the MACE method, enhancing surface recombination and external resistance. Consequently, the SHJ solar cell achieves a maximum PCE of 19.54% with UPs and 16.19% with IPs. After standardizing the geometric parameters (length, width, and tilt angle), optical simulations indicate that IPs outperform UPs only for incident angles smaller than 40°, with minimal influence of substrate thickness. Additionally, the light absorption advantage of IPs is further reduced or even negated when a rear reflective layer is applied to thin devices.

Supporting Information

Supporting Information is available from the Wiley Online Library or from the author.

Acknowledgements

This work was supported by the Major State Basic Research Development Program of China (grant no. 2022YFB4200101).

Conflict of Interest

The authors declare no conflict of interest.

Data Availability Statement

The data that support the findings of this study are available from the corresponding author upon reasonable request.

Keywords

inverted pyramids, optical simulation, resistance, silicon heterojunction solar cells, surface recombination

Received: March 10, 2025
Revised: March 11, 2025
Published online: April 11, 2025

[1] M. H. Shubbak, *Renew. Sust. Energy Rev.* **2019**, *115*, 109383.
[2] International Technology Roadmap for Photovoltaic, https://itrpv.vdma.org (accessed: December 2024).
[3] M. F. Abdullah, M. A. Alghoul, H. Naser, A. Nilofar, S. Ahmadi, Y. Sopian, *Renew. Sust. Energy Rev.* **2016**, *66*, 380.
[4] L. Zhu, S. Zou, M. Ni, J. Ding, C. Wu, Z. Lu, Y. Zeng, X. Ye, X. Wang, R. Fan, H. Sun, B. Liao, Y. Xu, M. Shen, X. Su, *Sol. RRL* **2022**, *6*, 2200204.
[5] H. Lin, M. Yang, X. Ru, G. Wang, S. Yin, F. Peng, C. Hong, M. Qu, J. Lu, L. Fang, C. Han, P. Procel, O. Isabella, P. Gao, Z. Li, X. Xu, *Nat. Energy* **2023**, *8*, 789.
[6] H. Wu, F. Ye, M. Yang, F. Luo, X. Tang, Q. Tang, H. Qiu, Z. Huang, G. Wang, Z. Sun, H. Lin, J. Wei, Y. Li, X. Tian, J. Zhang, L. Xie, X. Deng, T. Yuan, M. Yu, Y. Liu, P. Li, H. Chen, S. Zhou, Q. Xu, P. Li, J. Duan, J. Chen, C. Li, S. Yin, et al., *Nature* **2024**, *635*, 604.
[7] W. Liu, Y. Liu, Z. Yang, C. Xu, X. Li, S. Huang, J. Shi, J. Du, A. Han, Y. Yang, G. Xu, J. Yu, J. Ling, J. Peng, L. Yu, B. Ding, Y. Gao, K. Jiang, Z. Li, Y. Yang, Z. Li, S. Lan, H. Fu, B. Fan, Y. Fu, W. He, F. Li, X. Song, Y. Zhou, et al., *Nature* **2023**, *617*, 717.
[8] Y. Li, F. Peng, X. Ru, M. Qu, M. Yang, D. Chen, J. Xu, C. Xue, C. Yan, Y. Zheng, S. Yin, J. Lu, Z. Li, L. Fang, X. Xu, C. Hong, C. Su, Z. Shao, *Nature* **2024**, *626*, 105.
[9] W. Liu, H. Ma, A. Walsh, *Renew. Sust. Energy Rev.* **2019**, *116*, 109436.
[10] S. C. Baker-Finch, K. R. McIntosh, *Prog. Photovolt: Res. Appl.* **2011**, *19*, 406.
[11] Y. Jiang, H. Shen, T. Pu, C. Zheng, Q. Tang, K. Gao, J. Wu, C. Rui, Y. Li, Y. Liu, *Sol. Energy* **2017**, *142*, 91.
[12] Y. Fan, P. Han, P. Liang, Y. Xing, Z. Ye, S. Hu, *Appl. Surf. Sci.* **2013**, *264*, 761.
[13] H.-Y. Chen, H.-L. Lu, Q.-H. Ren, Y. Zhang, X.-F. Yang, S.-J. Dinga, Z. D. Wei, *Nanoscale* **2015**, *7*, 15142.
[14] L. Yang, Y. Liu, Y. Wang, W. Chen, Q. Chen, J. Wu, A. Kuznetsov, X. Du, *Sol. Energy Mater. Sol. Cells* **2017**, *166*, 121.
[15] K. Gao, Y. Liu, Y. Fan, L. Shi, Y. Zhuang, Y. Cui, S. Yuan, Y. Wan, W. Shen, Z. Huang, *Nanoscale Res. Lett.* **2020**, *15*, 174.
[16] J. Zhao, A. Wang, M. A. Green, *Sol. Energy Mater. Sol. Cells* **1994**, *32*, 89.
[17] J. Zhao, A. Wang, M. A. Green, *Prog. Photovolt: Res. Appl.* **1999**, *7*, 471.
[18] R. Tong, C. Li, S. Ma, X. Liu, S. Zou, D. Liu, *J. Mater. Sci. Mater. Electron.* **2023**, *34*, 54.
[19] Z. Sun, W. Chen, Y. Zhang, Y. Liu, X. Du, *Sol. Energy Mater. Sol. Cells* **2024**, *271*, 112867.
[20] S. M. Almenabawy, R. Prinja, N. P. Kherani, *Sol. Energy* **2023**, *256*, 88.
[21] D. Zhang, L. Wang, R. Jia, K. Tao, S. Jiang, H. Ge, B. Wang, Z. Gao, X. Li, M. Li, Z. Jin, *Mater. Sci. Semicond. Process.* **2022**, *138*, 106281.
[22] M. Moreno, D. Daineka, P. R. I. Cabarrocas, *Sol. Energy Mater. Sol. Cells* **2010**, *94*, 733.
[23] S. Almenabawy, Y. Zhang, A. Flood, R. Prinja, N. P. Kherani, *ACS Appl. Energy Mater.* **2022**, *5*, 13808.
[24] H.-P. Wang, A.-C. Li, T.-Y. Lin, J.-H. He, *Nano Energy* **2016**, *23*, 1.
[25] A. W. Smith, A. Rohatgi, *Sol. Energy Mater. Sol. Cells* **1993**, *29*, 37.
[26] Q. Chen, Y. Liu, Y. Wang, W. Chen, J. Wu, Y. Zhaoa, X. Du, *Sol. Energy* **2019**, *186*, 392.
[27] H. Tang, Y. Liu, Q. Chen, Y. Wang, W. Chen, J. Wu, Y. Zhao, X. Du, *ACS Appl. Electron. Mater.* **2019**, *1*, 2684.
[28] Q. Tang, H. Shen, H. Yao, K. Gao, Y. Jiang, Y. Li, Y. Liu, L. Zhang, Z. Ni, Q. Wei, *Renew. Energy* **2019**, *133*, 883.
[29] Q. Tang, H. Shena, H. Yao, K. Gao, J. Gea, L. Youwen, *Appl. Surf. Sci.* **2020**, *504*, 144588.
[30] A. Kumar, D. Rani, A. Saini, N. Joshi, R. K. Varma, M. Dutta, A. Samanta, *Sol. RRL* **2024**, *8*, 2400014.
[31] H. Xu, Z. Sihua, Y. Zhuangand, W. Shen, *Nanotechnology* **2018**, *29*, 015403.
[32] Y. Li, H. Sai, T. Matsui, Z. Xu, V. H. Nguyen, Y. Kurokawa, N. Usami, *Sol. RRL* **2022**, *6*, 2200707.
[33] C. Huo, J. Wang, H. Fu, X. Li, Y. Yang, H. Wang, A. Mateen, G. Farid, K.-Q. Peng, *Adv. Funct. Mater.* **2020**, *30*, 2005744.
[34] D. Du, H. Huang, X. Li, S. Ma, D. Zhao, R. Li, H. Huang, Z. Hao, F. Meng, L. Li, L. He, D. Ding, Z. Liu, W. Zhang, W. Shen, *Sol. RRL* **2024**, *8*, 2400052.
[35] M. A. Green, *Sol. Energy Mater. Sol. Cells* **2024**, *92*, 1305.
[36] D. Du, F. Qiao, Y. Guo, F. Wang, L. Wang, C. Gao, D. Zhang, J. Liang, Z. Xu, W. Shen, H. Wang, *Sol. Energy* **2022**, *245*, 146.
[37] D. Qiu, W. Duan, A. Lambertz, K. Bittkau, P. Steuter, Y. Liu, A. Gad, M. Pomaska, U. Rau, K. Ding, *Sol. Energy Mater. Sol. Cells* **2020**, *209*, 110471.
[38] H. Huang, D. Du, L. Li, C. Gao, S. Ma, X. Li, L. He, H. Su, D. Ding, Z. Li, W. Zhang, W. Shen, *Sol. Energy Mater. Sol. Cells* **2025**, *282*, 113392.
[39] C. Chen, S. Zheng, H. Song, *Chem. Soc. Rev.* **2021**, *50*, 7250.
[40] M. Y. Arafat, Y. A. Wahab, M. A. Islam, M. Hatta, M. R. Johan, N. E. Alias, H. Hussin, in *IEEE Int. Conf. on Semiconductor and Electronics*, IEEE, Piscataway, NJ **2024**, pp. 140–143.
[41] China PV Industry Development Roadmap, http://www.chinapv.org.cn (accessed: December 2024).
[42] A. Razzaq, T. G. Allen, W. Liu, Z. Liu, S. De Wolf, *Joule* **2022**, *6*, 514.